Soft Matter

PAPER

Realization of a stable, monodisperse water-in-oil droplet system with micro-scale and nano-scale confinement for tandem microscopy and diffusion NMR studies

Swomitra Palit, [ID] * Somayeh Khajehpour Tadavani [ID] and Anand Yethiraj [ID] *

In this work we generate stable and monodisperse water-in-oil emulsions using a co-flowing geometry that produced droplet sizes between 13 μm and 250 μm. The drops survived transfer to NMR tubes and were stable for at least 26 hours, enabling the performance of pulsed-field-gradient NMR experiments in addition to microscopy. The drops sizes achieved as a function of flow rate agree well with a simple model for droplet generation: this yields a precise measure of the interfacial tension. The design of a cell mimetic environment with nano-scale confinement has also been demonstrated with diffusion measurements on macromolecules (PEG and Ficoll70) within droplets that are further structured internally using agarose gel networks. Containing the agarose gel in droplets appears to provide very reproducible and homogeneous network environments, enabling quantitative agreement of Ficoll70 dynamics with a theoretical model, with no fit parameters, and, with PEG, yielding a systematic polymer-size dependent slowing down in the network. This is in contrast with bulk agarose, where identical macromolecular diffusion measurements indicate the presence of heterogeneities with water pockets.

1 Introduction

Diffusion in inhomogeneous media such as biological cells is complex because molecules encounter obstructing structures at both nano- and micro-scales.[1] In living cells the presence of the cytoplasm provides compartmentalization, crowding and above all a heterogeneous distribution of macromolecules.[2,3] *In vitro* compartmentalisation, using water-in-oil emulsions, is one system that can begin to mimic this complexity.[4] Encapsulation of macromolecules in microscopic water droplets is also powerful in that it enables the performance of laboratory operations using a fraction of the volume of reagents and significantly less time.[5,6]

Microfluidics offer opportunities for fundamental studies in cell biology.[7,8] In particular, it has been used for the generation of well-defined cellular microenvironments by encapsulating cells in droplets or microgels, followed by studies of cell growth and viability,[9,10] gene expression,[11] and enzymatic activity.[12] Hydrogels are an attractive starting point for re-creating the hierarchical structure of biological cells.[13,14] Agarose is a neutral polysaccharide that forms hydrogels at reduced temperatures.[15] It is extensively used in biomedical research because it is generally bio-inert, non-adsorptive to proteins and non-adhesive to cells, and its mechanical properties can be tuned

Physics and Physical Oceanography, Memorial University of Newfoundland, St. John's, NL, A1B 3X7, Canada. E-mail: swomitra@mun.ca, ayethiraj@mun.ca

by varying the agarose concentration in the gel.[16,17] While hydrogels can mimic nano-scale confinement, it is more challenging to generate robust and controlled multi-scale confinement spanning the nanometer and the micrometer scales.

The microfluidic encapsulation strategy has several important advantages: the ability to create 3D cellular microenvironments with precisely controlled dimensions, the capability to vary the properties of these environments at high throughputs of about 100 to 1000 highly monodisperse aqueous droplets per second.[18–20] However, it is not always obvious that these high-throughput strategies produce droplets that are stable when produced in the large quantities and for the long durations that are needed for small-angle scattering or nuclear magnetic resonance (NMR) spectroscopy. Thus, the challenge is to achieve long-time stability for droplets that can be loaded with macromolecules of choice and confining environments on the micro- and nano-scale.

One of the primary objectives of the current study is the generation of stable and monodisperse water-in-oil emulsions where we can incorporate micro-scale confinement *via* control of the water drop size, and nano-scale confinement by loading the drops with agarose gel, which forms a filamentous network that may be considered a physical, non-active analog of the cytoskeletal network.

In this study, the diffusion behaviors of two kinds of macromolecules – a flexible nonionic polymer, polyethylene glycol (PEG) and a compact uncharged polysaccharide

(Ficoll70) – are determined in three kinds of environments using pulsed-field-gradient NMR (PFG NMR), while employing, in tandem, the more rapid technique (optical microscopy) to ensure that the drops remain unchanged from production to NMR. The first environment is a simple water-in-oil emulsion which generates micro-scale confinement. The second environment is bulk agarose gel. The third is a water-in-oil emulsion where the aqueous phase is loaded with agarose gel: we refer to these as agarose gel microbeads. Using these three environments, we can examine the role of macromolecular diffusion in the presence of micro-scale confinement, nano-scale confinement, and a hierarchical micro- and nano-scale confinement. The significance of this work is that the results will enable a deep understanding of the diffusion behavior of these solutes in a biomimic system, which is needed for further progress in research of molecular diffusion *in vivo*.

2 Background

2.1 Stable and monodisperse micron-scale droplets

Using microfluidic technology, one can produce a uniform stream of droplets having diameters ranging from a few micrometres to hundreds of micrometres (corresponding to volumes between 0.5 pl and 4 nl) in a uniform, evenly spaced, continuous stream. Popular geometries for microfluidic droplet generation geometries are the T-junction, flow-focusing and the co-flow geometry. In the T-junction geometry, droplet formation occurs due to the combined effect of pressure changes in the continuous phase and the squeezing of the dispersed phase. This geometry is popular due to the ease with which droplets can be formed and the uniformity of the resulting droplets.[21,22] In flow-focusing microfluidics, the dispersed and continuous phases are forced through a narrow region in the microfluidic device. The design employs symmetric shearing by the continuous phase on the dispersed phase which enables more controlled and stable generation of droplets.[23,24] In a co-flowing geometry there are two concentric channels: the dispersed phase liquid is driven into the inner channel into parallel flowing stream of the continuous phase liquid. Co-flowing configurations result in highly monodisperse droplets with polydispersity values ranging from 1% to 2%. The droplet sizes produced range from as small as 80 μm up to a few hundred micrometres in diameter.[25,26]

Making stable water-in-oil emulsions is challenging. Emulsions can be stabilized by amphiphilic surfactants and surface-active polymers,[27] colloidal particles,[28] or a combination of particles and surfactants.[29] In surfactant-stabilized emulsions, the HLB value, which is a measure for the ratio of hydrophilic to hydrophobic parts of the surfactant, is often considered to classify low-molecular-weight amphiphiles, while the main factor influencing the ability of colloidal particles to form so-called Pickering emulsions is the particle-surface wettability.[28]

2.2 Agarose gel and nano-scale confinement

For a macromolecule in dilute solution, the Stokes–Einstein relation,

$$D_0 = \frac{k_B T}{6\pi\eta R_H},\qquad(1)$$

relates the self-diffusion coefficient D_0 with the hydrodynamic radius, R_H, and the solvent viscosity, η.

Agarose gel is an irregular 3D matrix of fibers filled with water.[30] A solute can diffuse freely in the water, but in agarose it will be impeded by the fibers. The arrangement of the fibers in the matrix also has an effect on the magnitude of steric interaction. An ordered arrangement of fibers impedes diffusion less than a disordered or random arrangement, as is found in agarose.[31]

The relationship between the hydrodynamic radius of a solute and the pore size of a fibrous medium plays a large role in how the solute is able to diffuse in such a medium. The pore size describes the amount of space between the fibers that make up the medium. It is well known that the mesh sizes in polymer hydrogels depend on the volume fraction, Φ, or mass fraction μ (in agarose $\mu = 1.025\Phi$), of polymeric material in solution: this is also referred to as the fiber density. There is wide variance in pore size, from 1 nm to 900 nm.[32–40] A smaller pore size results from a higher fiber density (higher μ or Φ) and results in a greater hindrance to diffusion. Typical mass fractions for agarose gel range from 0.5% to 7.5%.

In general, the relative diffusivity (the diffusivity in the gel divided by the corresponding aqueous value in unconfined water) is found to decrease as molecular size and/or gel polymer concentration are increased. One way to describe the effects of molecular size is to use hindered transport theories developed for membranes with long, regularly shaped (such as cylindrical) pores.[41] Thus, a given gel might be viewed as having a certain effective pore size and pore number density. However, there is no clear way to predict those pore parameters from actual compositional variables, such as the volume fraction of cross-linked polymer. Closer to reality are models that envision a gel as a network of polymeric fibers with fluid-filled interstices. In such models, it is usually assumed that a single type of rigid, cylindrical fiber is arranged in either a random or spatially periodic array. Thus, a given gel might be viewed as having a certain effective pore size and pore number density. Ogston *et al.* proposed a stochastic model for the hindered diffusion coefficient of a solute molecule in a random fiber matrix.[42] They assumed that a single type of rigid, cylindrical fiber is arranged in either a random or spatially periodic array, and that the hindered mobility is due to steric obstructions of the fibers. In their picture, the reduced diffusion coefficient, D_g/D_0, is equal to the probability of a random-walk step of the test particle without collision. The derived expression for the reduced diffusion coefficient is

$$\frac{D_g}{D_0} = \exp\left(-\frac{(R_H + R_f)}{R_f}\Phi^{0.5}\right),\qquad(2)$$

where Φ represents the volume fraction of the polymer, R_H the hydrodynamic radius of the diffusing molecule and R_f defines the effective cylindrical radius of the fiber. A recent experimental work on dextran molecules diffusing as probe through a polyacrylamide hydrogel shows excellent agreement with Ogston model.[43] However, the Ogston model is sometimes unsatisfactory for agarose gels, overestimating the influence

of polymer concentration on the diffusion coefficients in cases where the proteins and polymeric macromolecules are flexible in structure.[44,45]

NMR relaxation measurements can also be used to get information about pore size. D'Agostino et al.[46] measured the change in relaxation rate with gel concentration. The relaxation rate is expected to depend linearly on the surface–volume ratio, so they used the relation

$$\Delta\left(\frac{1}{T_1}\right) \equiv \frac{1}{T_1(\Phi_A)} - \frac{1}{T_1(\Phi_A = 0)} = \frac{2}{R_{pore}}\rho, \qquad (3)$$

where $\frac{2}{R_{pore}}$ is the surface-to-volume ratio assuming that the pores are cylindrical in shape with a pore radius R_{pore}; ρ is a material property known as the surface relaxivity.

3 Method

3.1 Droplet generation

The liquids we employ were deionized water as the aqueous phase, and mineral oil (Fisher Scientific, CAS 0122B-4) with a density of 870 kg m^{-3} and dynamic viscosity of 32×10^{-3} Pa s as the oil phase. A non-ionic surfactant span-80 (Sigma-Aldrich) was added into the 100 ml oil phase at 4.5% (v/v) as a surfactant. The resulting oil–surfactant mixture was stirred on a magnetic stir plate for an hour.

As shown in Fig. 1, the experimental device used in this work is made of two coaxially aligned cylindrical capillary tubes. The inner capillary tube with a tip tapered to an inner diameter, D_{tip}, of (15 ± 0.2) μm, (19 ± 0.4) μm, and (26 ± 0.5) μm; and an outer diameter $D_{out} = 1.2 \pm 0.2$ mm. The coaxial alignment of the tubes is achieved by matching the outer diameter of the untapered portion of the inner capillary to the inner dimension of the outer capillary.

In all the experiments reported here, the generation of droplets of variable size is achieved by changing both the inner capillary diameter (D_{tip}) as well as the oil flow rate (Q_{oil}). The inner fluid is deionized water and the outer fluid is mineral oil (with Span80), which leads to water drops that form in a continuous phase of oil. Both liquids are injected through syringe pumps. In this study, the experiments are performed
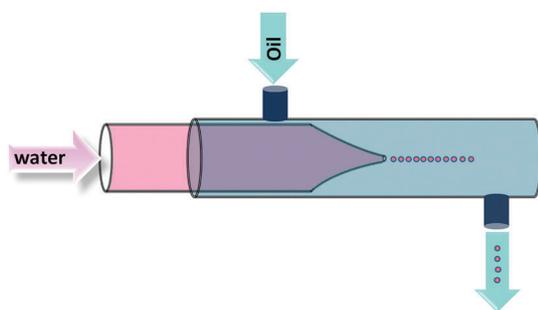
Fig. 1 Droplet formation: schematic of production of water-in-oil emulsion droplets in microfluidic device with coflowing geometry.

at constant dispersed phase flow rate ($Q_{water} = 0.001$ cm^3 min^{-1}), where Q_{oil} is always much greater than Q_{water}.

The measured size distribution of droplets remained unchanged for the maximum measured duration of 26 hours. However, the water-in-oil droplets were breaking into smaller droplets while transferring from the production container to the NMR tube. Several methods had been used to prevent droplet break up. The idea of adding 1% (w/v) hydrophobic fumed silica nanoparticles (Aerosil @ R972, Evonik, with a mean particle diameter of 16 nm[47]) with mineral oil proved to be the most effective. The silica nano-particles form a thin layer around the water droplets and provide better stability against break up. Measurements for simple micro-scale confinement reported in this article are therefore for the silica particle stabilized water-in-mineral oil emulsion. As also stated in the next sub-section, introducing nanoscale confinement in the form of agarose gel was itself adequate to drop stability, and in that case, nano-particle stabilization was not necessary.

3.2 The NMR self-diffusion measurement

Pulsed field gradient nuclear magnetic resonance (PFG-NMR) is a common non-invasive technique to study the size distribution and dynamics of single emulsion systems with advantages that it can be used on concentrated opaque emulsions and is a non-destructive technique.[48,49] PFG NMR measurements were carried out on a Bruker Avance II 600 spectrometer equipped with a Bruker 14.08 T magnet, and a Bruker diffusion Diff30 probe (with a ^{1}H radiofrequency coil insert with an inner diameter of 5 mm) with a maximum Z gradient strength of 30 G cm^{-1} A^{-1}. The spectrometer was also equipped with a (60 A maximum current) gradient amplifier and thus a maximum gradient of 1800 Gauss cm^{-1} (18 T m^{-1}). To avoid probe heating and to control sample temperature, the probe was cooled by flowing water and the temperature maintained at 25 °C. We use a pulsed-field-gradient stimulated echo pulse program to measure diffusion.[50] The gradient steps were varied and the signal for H$_2$O, PEG of different molecular weight and Ficoll70 were collected as a function of gradient. Signal attenuation due to diffusion in the stimulated echo sequence is given by

$$S(g) = S_0 \exp(-\gamma^2 g^2 \delta^2 (\Delta - \delta/3)D), \qquad (4)$$

where $S(g)$ is the intensity of the signal in the presence of field gradient pulse, $S(0)$ is the intensity of the signal in the absence of field gradient pulse, $\gamma = \gamma^H = 2.657 \times 10^8$ T^{-1} s^{-1} is the proton gyromagnetic ratio, $\delta = 2$ ms is the duration of field gradient pulse, $\Delta = 500$ ms is the time period between two field gradient pulses, and g is the amplitude of field gradient pulse.

Also, for agarose gel, we measured longitudinal relaxation time (T_1) values from a series of spectra collected using a standard inversion-recovery pulse sequence.

3.3 Restricted diffusion and the droplet size distribution

Diffusion of molecules inside a cavity is known as "restricted diffusion". As the molecules inside the cavity are not diffusing freely, the behavior of signal attenuation is different from that of unrestricted diffusion. Callaghan et al. used pulsed-field

gradient spin echo experiment to measure the diffusion coefficients of water and fat in Cheddar and Swiss cheeses.[48] They considered a cheese matrix as a collection of droplets with a Gaussian distribution of sphere volume. The resulting echo attenuation was

$$S(g) = S_0 \exp\left(-\alpha^2 a_0^2 \left[1 + \sigma^2\alpha^2\right]^{-1} - \frac{1}{2}\ln\left[1 + \sigma^2\alpha^2\right]\right), \quad (5)$$

where a_0 is the mean radius and $\sigma/\sqrt{2}$ is the standard deviation. The variable α^2 depends on the gradient strength and gradient pulse duration, $\gamma^2 g^2 \delta^2$. The above expression is valid for the condition $\exp(-a_0^2/\sigma^2) \ll 1$.

3.4 Optical microscopy and characterization

In this work, a Nikon Eclipse 80i upright optical microscope was used. A high speed camera (model PCO.Edge) was mounted on the microscope rear port. Bright field microscopy was used to measure the emulsion size and stability. The size distribution of droplets was analyzed using a computer program that was coded in Interactive Data Language (IDL).

4 Results: achieving stable confinement

In this work we generated stable, monodisperse water-in-oil emulsion with micro-scale and nano-scale confinement.

4.1 Preparation of micro-scale confinement

As shown in Fig. 2 (see also Appendix Fig. 9), our microfluidic system demonstrates a high degree of versatility in the size of droplets produced. By varying Q_{oil}, a wide range of droplet sizes (14 μm to 265 μm) was produced with excellent size selectivity: a summary of results is shown here for silica-nanoparticle stabilized suspensions (with details in the Appendix). We find that a decrease in the rate of flow of the continuous phase increases the size of the droplets – a phenomenon consistent with previous studies.[23,51] We observe that the channel dimension governs the size of the water droplet. With a smaller inner capillary dimension, smaller droplets are generated. This is because the higher flow rate in the smaller channels increases the shear rate in the system, resulting smaller droplets.

For small inner fluid flow rates, following Umbanhowar et al.,[25] we may write an equation relating the droplet size
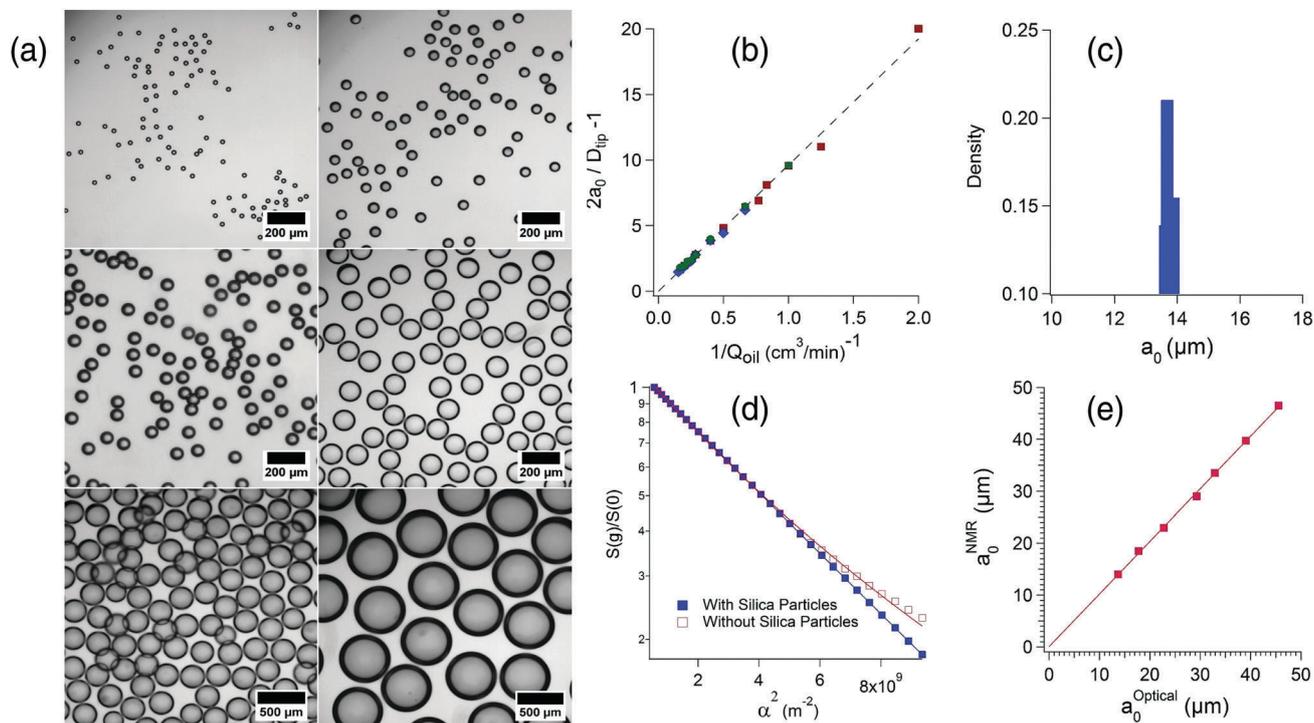
Fig. 2 Stable and monodisperse droplets: monodisperse water-in-oil emulsion of different droplet sizes are generated in microfluidic device. These droplets were verified to be stable for at least 26 hours. (a) Droplet radius are: (13.7 ± 0.2) μm; (23.2 ± 0.4) μm using D_{tip} = (15 ± 0.2) μm (top), (38.2 ± 0.4) μm; (59 ± 1) μm using D_{tip} = (19 ± 0.4) μm (middle), (126 ± 3) μm; (265 ± 4) μm using D_{tip} = (26 ± 0.5) μm (bottom). (b) Flow curve for droplet diameter, normalized by the tip diameter (D_{tip}) of the inner capillary, as a function of the external oil flow rate. Here the dashed line has a functional form of $2a_0/D_{tip} - 1 = b/Q_{oil}$ that is consistent with the form suggested by Umbanhowar et al.[25] The agreement is excellent, with the one fit parameter b = (9.7 ± 0.1) cm³ min⁻¹. (c) Using optical microscopy and image-processing methods (see text), the mean radius of the water droplets in silica nanoparticle stabilized mineral oil was measured. For example, the droplets in figure (a) (top left) had a size distribution yielding (13.7 ± 0.2) μm. (d) PFG NMR signal attenuation of water. From the fit (blue line) the droplet radius was measured (14 ± 0.5) μm. In case of water in oil emulsion without silica nanoparticles, from the fit (red line), droplet radius was measured (14 ± 6) μm. (e) Comparison of mean droplet diameter (using silica nanoparticle stabilization) obtained by PFG NMR and microscopy. In all cases shown, the drops were stabilized with silica nanoparticles, as described in the text.

$(2a_0)$ (scaled by the inner diameter, D_{tip}, of the capillary tube) to the velocity v of the continuous phase:

$$\frac{2a_0}{D_{tip}} = 1 + \frac{v_s}{v}.$$

In this equation $v_s = \gamma/3\eta_c$, where γ is the interfacial tension and η_c is the viscosity of the continuous phase. By introducing the cross-sectional area of the outer channel $(\pi(D_{out}/2)^2)$ one can write the above equation as

$$\frac{2a_0}{D_{tip}} - 1 = \frac{\pi(D_{out}/2)^2 \frac{\gamma}{3\eta_c}}{Q_{oil}} = \frac{b}{Q_{oil}}, \quad (6)$$

where $b = \pi(D_{out}/2)^2 \frac{\gamma}{3\eta_c}$.

Experiments were performed using three different tip diameters (D_{tip}): (15 ± 0.2) μm, (19 ± 0.4) μm, and (26 ± 0.5) μm. The resulting drops, imaged with a microscope, are shown in Fig. 2(a) (the top, middle and bottom panels refer to (D_{tip} = (15 ± 0.2) μm, (19 ± 0.4) μm, and (26 ± 0.5) μm respectively)). A complete set of drop sizes generated is shown in the Appendix (Fig. 9). The resulting drop radii a_0 are shown as a function of Q_{oil} in Fig. 10 (Appendix). In Fig. 2(b), the plot of $2a_0/D_{tip} - 1$ against $1/Q_{oil}$ collapses all the results of drop sizes onto one master curve that is remarkably linear and thus in agreement with eqn (6), with a fitted $b = (9.7 \pm 0.1)$ cm³ min⁻¹. Knowing D_{out} = 12 mm and the measured value of viscosity η_c = 0.05 Pa s, we calculate the interfacial tension between water and nanoparticle–mineral oil suspension: $\gamma = 21 \pm 0.3$ mN m⁻¹. The reported value of water–mineral oil interfacial tension is about 50 mN m⁻¹.[52,53] So, the addition of nanoparticles reduces the interfacial tension which is consistent with expectations;[54] in addition, due to the good agreement with the model function,[25] we obtain a rather precise determination of the interfacial tension in this system.

Next, we transferred these water-in-oil suspensions into NMR tubes for PFG NMR studies. In Fig. 2(d), the signal attenuation of water-in-oil droplets, whose mean radius was determined by microscopy (Fig. 2(c)) to be (13.7 ± 0.2) μm, was plotted as a function of α^2, the gradient variable in eqn (5).

We used eqn (5) in order to determine the droplet size distribution for both cases: with and without silica particles dispersed in oil phase. From the fit, the mean droplet radius $a_0 = (14 \pm 6)$ μm for the system without silica particles. On the other hand, the addition of silica particles (Fig. 2(d), solid blue line) as Pickering stabilizers dramatically reduced the width of the droplet size distribution: here, $a_0 = 14 \pm 0.5$ μm. This difference was seen systematically in two trials. Hence, water drops that are monodisperse upon production (and thus during sizing by microscopy) not only break into smaller droplets, but also coalesce into larger ones during the transfer to the NMR tube, but this broadening of the size distribution is mitigated by Pickering stabilization.

We show, in Fig. 2(e) that droplet radii, as determined by NMR in a single ensemble measurement, correlate very well with those determined painstakingly by microscopy. This reassures us that the droplet systems that we generate, and characterize using microscopy are not changed upon loading into NMR tubes for long-time experiments.

4.2 Preparation of nano-scale confinement

We used eight different molecular weights of PEG (8000 to 5 000 000), purchased from Alfa Aesar. Ultra-low gelling agarose and Ficoll PM 70 (referred to as Ficoll70 in the text) with average molecular weight of 70 000 (mean radius, R_H = 5.5 nm[55]) were purchased from Sigma Aldrich.

Agarose gels with different agarose concentrations were prepared in a series of steps. The desired weight of ultra-low gelling temperature agarose purchased from Sigma Aldrich was added to distilled water, and then the mixture was heated to the boiling temperature of the solution for complete dissolution of the agarose. Ficoll70 and PEGs were mixed into the agarose solution before gelation. The volume fraction of agarose in the gel was calculated with a density of dry agarose powder (1.64 g cm⁻³) and a mass fraction of agarose in the agarose gel fiber (0.625) according to Pluen's method.[38]

Uniform-sized agarose microbeads were prepared by the microfluidic technique in this study. A mixture of agarose gel with Ficoll70/PEG was used as the aqueous phase. Agarose-loaded drops did not need the additional silica nanoparticle stabilization. Both the liquids were driven through the capillaries by syringe pumps. We choose ultra-low gelling agarose, which has a gelling point of around 16 °C. Once melted, this agarose will remain in the liquid phase until the temperature drops below 16 °C, which ensures easy generation of agarose droplet under room temperature. Uniform agarose microbeads in oil were cooled to 4 °C for 23 hours. When the temperature dropped to 4 °C, agarose emulsion droplets solidified.

We generated agarose microbeads (Fig. 3) of two different diameters $2a_0$, using the microfluidic device, for our studies of nanoscale confinement: $2a_0 = (283 \pm 6)$ μm and $2a_0 = (561 \pm 8)$ μm. For the results reported, we used (561 ± 8) μm microbeads.

5 Results: self-diffusion

5.1 Microscale confinement: diffusion of PEG polymer

Polyethyleneglycols (PEG) have been selected as model solutes to study the effects of confinement. This offers a series of key
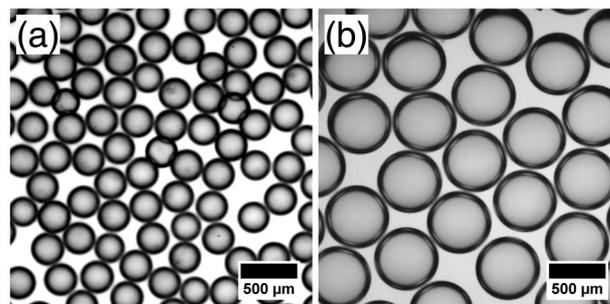
Fig. 3 Introducing nano-scale confinement: agarose microbeads with diameter (a) $2a_0 = (283 \pm 6)$ μm and (b) $2a_0 = (561 \pm 8)$ μm generated by the microfluidic device.
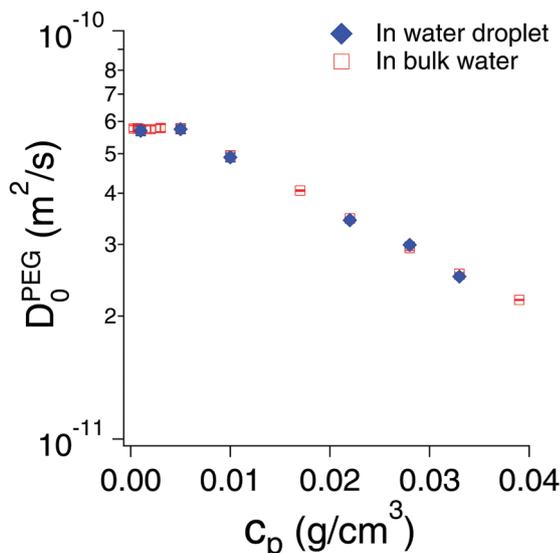
Fig. 4 Micro-scale confinement is essentially bulk for PEG: self-diffusion coefficient of PEG (M_w = 20 000) as a function of polymer concentration c_p in bulk water (red squares) as well as in water droplets of radius a_0 = (14 ± 0.5) μm (blue diamonds): there is no discernible difference. The diffusion time, $\Delta < a_0^2/2D_0^{PEG}$, and therefore, PEG chains do not experience the confinement.

Fig. 5 Dynamics of spherical macromolecule in gel: diffusion coefficients of Ficoll70 (Φ_F = 0.02) for several volume fractions Φ_A of agarose gel both in bulk and microbead. Diffusion coefficients of Ficoll70 in agarose gel microbeads agrees reasonably well with Ogston model (green dashed line).

advantages: a broad range of molecular weights can be covered, within the same family of unbranched, highly flexible macromolecules. A polydispersity factor close to unity is achievable within this family of macromolecules which prevents complications arising from molecular weight distribution effects. Moreover, the fact that water is a good solvent of PEG at room temperature ensures a behaviour in solution that is relatively easy to predict. Fig. 4 presents the self-diffusion coefficient of PEG (M_w = 20 000, R_H = 4.8 nm) as a function of polymer concentration c_p in bulk water (red squares) as well as in water droplet (blue diamonds). In recent work, we found that the polymer self-diffusion coefficient exhibits a plateau below a characteristic polymer concentration and in a crossover region between the dilute and semidilute regime, there is an exponential decrease in the long-time self-diffusion coefficient with polymer concentration.[56] This behaviour is seen here as well, but what Fig. 4 shows is that the diffusion of PEG in a bulk water is indistinguishable both qualitatively and quantitatively from that of PEG in the water droplet. This is not surprising: the diffusion time Δ is much less than $(a_0)^2/2D_0^{PEG}$, where a_0 is the radius of the droplet and D_0^{PEG} is the diffusion coefficient of the PEG molecules at infinite dilution. Thus, the PEG chains spend a very small fraction of their time near the droplet surface. This reassures us that the PEG is uniformly distributed within the drop and not associating strongly at the drop surface.

5.2 Nanoscale confinement: diffusion of Ficoll70 spheres

Polymers have the ability to deform in order to go through nanopores. Diffusion models for macromolecules in gel network use the radius of the solute (R_H) in their predictive computations. This hard sphere analogy can be worthwhile
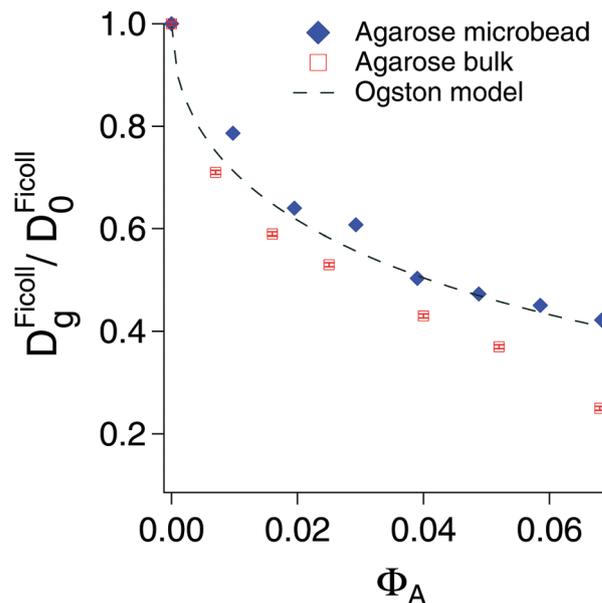
for the diffusion of a spherical polysaccharide (e.g. Ficoll70) but is unlikely to hold for chain molecules. Thus, we begin by quantitatively examining the experimental self-diffusion of Ficoll70 (which have a compact spherical shape) in agarose gels, which provide the nanoscale confinement, both without ("bulk") and with ("bead") the micro-scale confinement.

Diffusion coefficients of Ficoll70 in H_2O and inside the agarose gel were extracted from the NMR measurements using eqn (4) to fit the echo amplitudes. Fig. 5 presents the dependence of the diffusion coefficients of Ficoll70 on the volume fraction (Φ_A) of agarose gel. A systematic decrease in diffusion coefficients is observed as a function of increasing agarose volume fraction in the gels. A decrease is, of course, expected and can be attributed to the fact that the increase in the volume fraction of agarose in the gels reduces the space for the diffusion of Ficoll70. It is also consistent with previous measurements.[57–60]

Here, however, we make quantitative connection with a theoretical model.

The dashed lines in Fig. 5 represent the curve calculated with the Ogston model (eqn (2)) using a particle hydrodynamic radius R_H = 5.5 nm and the previously determined agarose gel fibre cylinder radius R_f = 1.9 nm.[61,62] This is especially notable because the model is overlaid atop the data, with no free parameters.

What is also notable is that, while the agreement of the Ogston model is excellent for the system with hierarchical nanoscale and micro-scale confinement (agarose in microbeads), it is less predictive for diffusion in bulk agarose. This suggests that producing gel-loaded microbeads might provide a more homogeneous gel environment, and is an issue we examine next.

5.3 Water dynamics: bulk *versus* microbead agarose

The reductions in Ficoll70 diffusivities in agarose microbeads as a function of Φ_A are well described by Ogston model. But why is the dynamics of Ficoll70 different for bulk agarose? Water dynamics allows us to explore this further.

Fig. 6 shows the self-diffusion of water in agarose gel, both in bulk (Fig. 6(a)) and in microscale beads (Fig. 6(b)), as a function of agarose volume fraction Φ_A. A linear decrease of D_w with Φ_A was found in both bulk and microbead environments. This likely can be ascribed to previous findings[63] that the number of water molecules interacting with hydroxyl groups of agarose gel, through mechanisms including hydrogen bonding and chemical exchange of protons, depends on the volume fraction of the agarose.

However, what is the most remarkable finding is highlighted in Fig. 6(c): the self-diffusivity in bulk agarose is nearly a factor of 100 larger than that for microbead agarose, when in principle, the two should be identical!

Another way to probe water dynamics is *via* relaxation rate measurements.[46] We observe in Fig. 7(a) and (b) that the
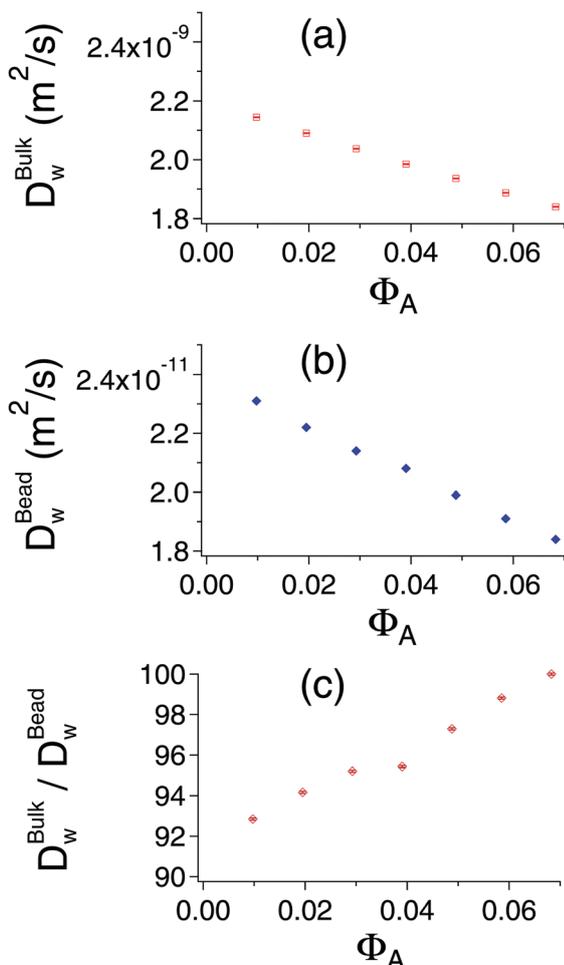
Fig. 6 Dynamics of water in gel: diffusion coefficients of water as a function of volume fractions for agarose gel (Φ_A) in (a) bulk and (b) microbead. (c) Ratio of self-diffusion coefficients of water in bulk and microbeads as a function of Φ_A. This ratio increases linearly with Φ_A.

longitudinal relaxation rate ($1/T_1$) of hydrogen atoms of water increased with agarose gel volume fraction. The increase with Φ_A is linear in both bulk and microbead agarose environments (with intercepts of (0.27 ± 0.001) s^{-1} and (0.48 ± 0.006) s^{-1} for bulk and microbead agarose, respectively) and is consistent with the model represented by eqn (3). The intercept for bulk agarose corresponds to the relaxation rates of pure water ($1/T_1(\Phi_A = 0)$) at 25 °C.

In Fig. 7(c) we plot the difference $\Delta(1/T_1) \equiv \frac{1}{T_1(\Phi_A)} - \frac{1}{T_1(\Phi_A = 0)}$ for both bulk and agarose microbead against Φ_A: one sees a proportional relationship with respect to Φ_A, but with very different (a factor of 4) slopes. Eqn (3) predicts a proportional relationship of $\Delta(1/T_1)$ with the surface-to-volume ratio, so this implies that the surface-to-volume ratio is proportional to Φ_A.

Regardless of pore geometry, $\Delta(1/T_1)$ will always be inversely related to pore radius, and we can thus extract relative pore radii as a function of Φ_A. In Fig. 7(d), we plot a relative pore radius $P(\Phi_A) \equiv R_{pore}/R_{pore}(\Phi_A = 0.02)$, and this relative radius shows a very similar dependence for bulk and microbead agarose.

Finally, we can obtain numerical estimates of R_{pore} as a function of Φ_A using the $P(\Phi_A)$ shown in Fig. 7(d) and tabulated in Table 1 (Appendix), along with the literature values of pore radius for isolated samples. The pore radius reported for bulk agarose, for a sample at $\Phi_A = 0.02$, is (103 ± 13) nm,[38] while for a microbead sample reported in the literature at $\Phi_A = 0.04$, it is (120 ± 2) nm.[64] For bulk agarose, we obtain $R_{pore}^{bulk}(\Phi_A)$ using $R_{pore}^{bulk}(\Phi_A) = P^{bulk}(\Phi_A) \times 103$ nm while for microbead agarose, we can obtain $R_{pore}^{bead}(\Phi_A)$ using $R_{pore}^{bead}(\Phi_A) = \frac{P^{bead}(\Phi_A)}{P^{bead}(\Phi_A = 0.04)} \times 120$ nm. At $\Phi_A = 0.02$, for example, this yields $R_{pore}^{bead} = 230$ nm.

We hypothesize at this point that one reason for discrepancy in water dynamics could be that the pore sizes are more regular in the microbeads, and more heterogeneous in the bulk agarose with large water pockets that behave essentially like bulk water. In order, to examine this hypothesis we measured, next, the diffusivities of different molecular weights of PEG in agarose gel. If the pore size is regular, one should see a clear decrease in the diffusivity of PEG, relative to its bulk water value, as its hydrodynamic size approaches the agarose network pore size.

5.4 Diffusion of PEG in agarose gel: bulk *vs.* microbeads

As shown in Fig. 4, dynamics of PEG is insensitive to microscale confinement. Here, we examine the introduction nanoscale confinement, *via* the agarose gel network. Once again, we compare self-diffusion in bulk agarose with that in microbeads.

The diffusion coefficients for PEGs in water ($D_0^{PEG}(0,M_w)$) and in agarose gel ($D_g^{PEG}(\Phi_A,M_w)$) are measured by the PFG NMR method, at a polymer concentration $c_p = 0.005$ g cm^{-3} that is in the dilute limit. We define the ratio of the PEG diffusivity in agarose gel to that in water at dilute solute concentrations as:

$$\Lambda(\Phi_A,M_w) = D_g^{PEG}(\Phi_A,M_w)/D_0^{PEG}(0,M_w). \qquad (7)$$
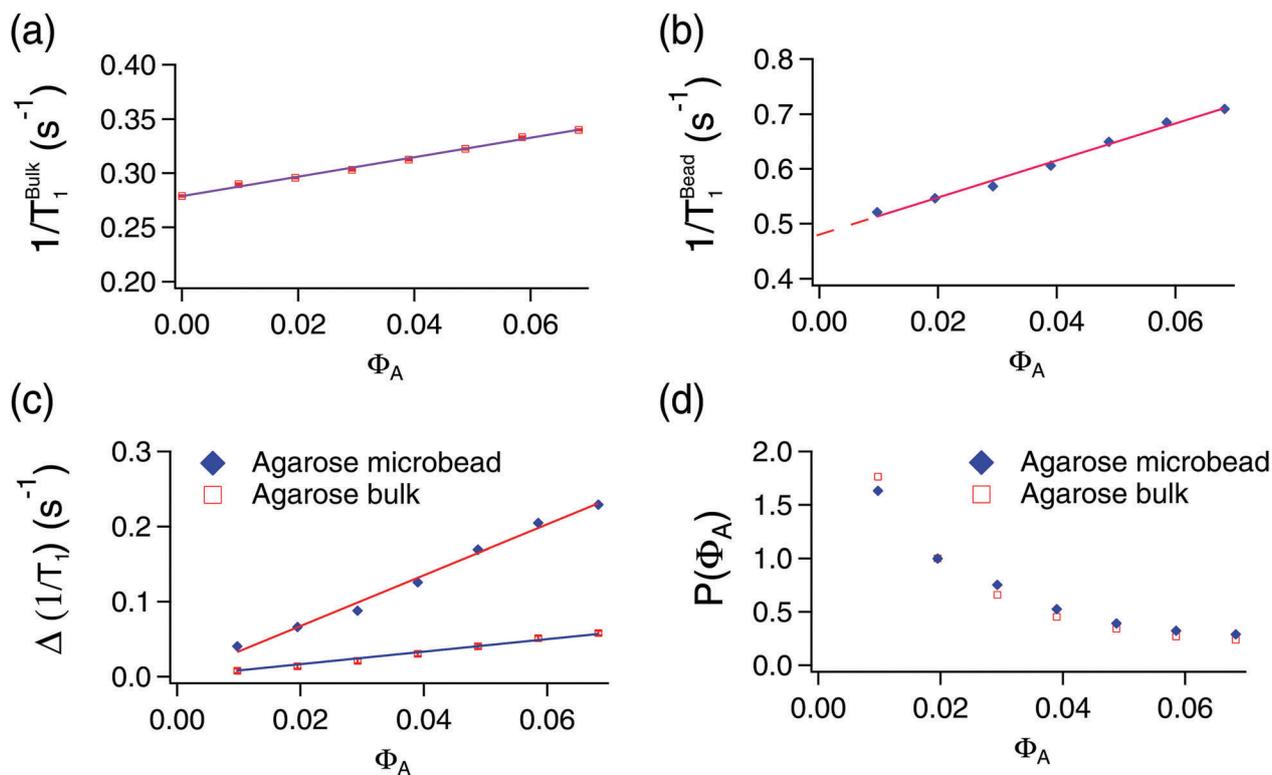
Fig. 7 Relaxation rate and pore radius: relaxation rates of water as a function of volume fractions for agarose gel (Φ_A) in (a) bulk and (b) agarose microbead, (c) difference in longitudinal relaxation rate, $\Delta\left(\dfrac{1}{T_1}\right)$ for both bulk and agarose microbead, (d) $P(\Phi_A)$, pore radius (relative to its value at $\Phi_A = 0.02$) as a function of agarose gel volume fractions, Φ_A.

Table 1 $P(\Phi_A) \equiv R_{pore}/R_{pore}(\Phi_A = 0.02)$ for different volume fractions of bulk and agarose microbeads

$P(\Phi_A)$		
Volume fraction (Φ_A)	Agarose bulk	Agarose microbead
0.01	1.76	1.63
0.02	1	1
0.03	0.66	0.75
0.04	0.45	0.53
0.05	0.34	0.39
0.06	0.27	0.32
0.07	0.24	0.29

In Fig. 8(a), $\Lambda(\Phi_A, M_w = 20\,000)$ is not at all in agreement with the Ogston model, but in fact is more mobile than the predicted value, consistent with the fact that PEG is a flexible chainlike molecule.

Next, in Fig. 8(b), we show the diffusion coefficient of PEGs in agarose gel ($D_g^{PEG}(\Phi_A = 0.02, M_w)$) in both microbeads (blue diamonds) and in bulk agarose (red squares). Shown for comparison is the corresponding diffusion coefficient $D_0^{PEG}(0, M_w)$ in pure water, with no confinement (grey circles). The polymer hydrodynamic radius R_H is calculated with eqn (1) from $D_0^{PEG}(0, M_w)$: for M_w ranging from 8000 to 5 000 000, R_H ranged from 2.2 to 73 nm. The diffusion coefficients of PEG in the gel decrease with an increase in the molecular weight of PEG both for bulk agarose and agarose in microbeads. However, there is a clear scaling behaviour for unconfined PEG

(in water) and for PEG in microbeads. If the diffusion follows Zimm dynamics, that is, the interior volume of the polymer behaves like a solid diffusing object, then, the relationship between M_w and the diffusion coefficient in a dilute solution, $D_0^{PEG}(0, M_w)$, can be expressed as[65]

$$D_0^{PEG}(0, M_w) = kM_w^{-\nu}, \qquad (8)$$

where k is a pre-factor related to the segment size of the polymer chain and ν is a scaling exponent that depends on the polymer–solvent system. From a linear fitting of the plot of $D_0^{PEG}(0, M_w)$ and $D_g^{PEG}(\Phi_A, M_w)$ in agarose microbead with respect to M_w, ν is obtained to be 0.54 ± 0.01 for PEG in dilute aqueous solution and 0.53 ± 0.01 for PEG in agarose microbeads.

Fig. 8(c) highlights the difference between agarose bulk vs. microbead by showing $\Lambda(\Phi_A = 0.02, M_w)$ for both environments. We find both ratios converging for the largest molecular weights, but the key observation is that while $\Lambda(\Phi_A = 0.02, M_w)$ is independent of M_w for the microbead environment, it increases with M_w for bulk agarose.

As shown by Monte Carlo simulation of molecular diffusion in gels, this ratio would be expected to depend on the ratio of the radius of the macromolecule and agarose gel pore radius (R_H/R_{pore}) for $R_H/R_{pore} > 0.2$.[66] For $\Phi_A = 0.02$, the calculated value of pore radius is 230 nm for agarose microbead. While we do probe polymer sizes from $R_H = 2$ nm to 70 nm, we observe no
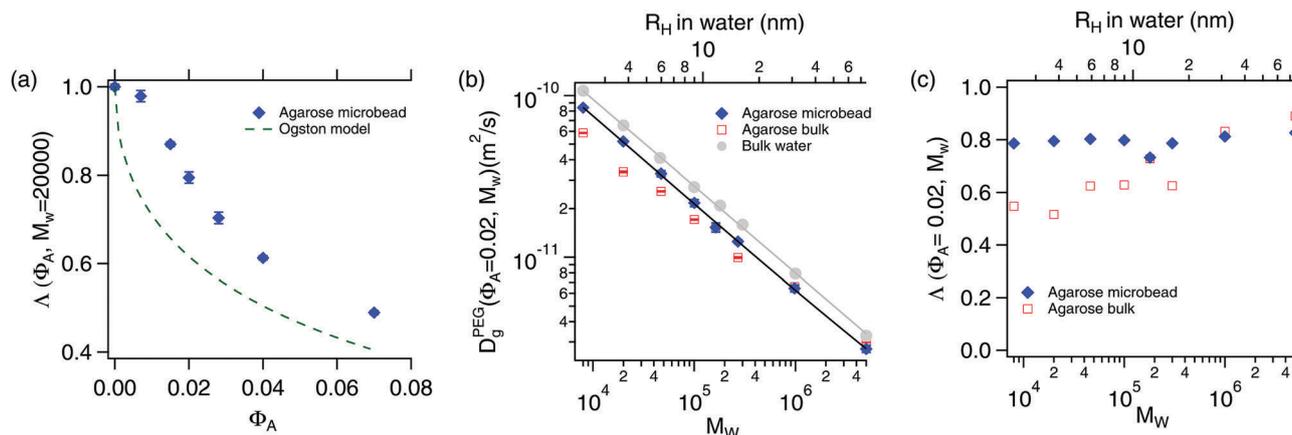
Fig. 8 Dynamics of chain macromolecule in gel: (a) relative diffusivity of PEG ($\Lambda(\Phi_A, M_w = 20\,000)$) of $c_p = 0.005$ g cm^{-3} in agarose microbeads do not agree with Ogston model (green dashed line). (b) Diffusion coefficients of PEG in agarose gel ($D_g^{PEG}(\Phi_A, M_w)$) as a function of molecular weight (M_w) both for bulk and microbead form. Here the diffusion coefficients of PEG in bulk water ($D_0^{PEG}(0, M_w)$) are shown in grey. From the power law fit ($D_0^{PEG}(0, M_w) = k M_w^{-\nu}$), ν is obtained to be 0.54 ± 0.01 for PEG in dilute aqueous solution and 0.53 ± 0.01 for PEG in agarose microbeads. (c) The relative value of PEG diffusion coefficients in agarose gel (D_g^{PEG}) compared to those in solution (D_0^{PEG}) are plotted as a function of molecular weight (M_w). This ratio is independent of M_w for the microbead environment but increases with M_w for bulk agarose. The corresponding hydrodynamic radius (R_H) for equivalent spheres as estimated by the Stokes–Einstein equation is shown for reference. In (b) and (c) the volume fraction of gel, $\Phi_A = 0.02$ and $c_p = 0.005$ g cm^{-3}.

dependence of R_H in this range for microbead. Experiments are planned for larger R_H.

6 Discussion and conclusions

In this work, we have successfully generated a system with hierarchical micro-scale and nano-scale confinement. We are able to generate water-in-oil systems (without and with nano-scale confinement) that are stable with respect to transfer and over a period of days.

While micro-scale confinement is not expected to directly induce confinement for large macromolecules, because of the large diffusion times, there is, however, a more subtle effect. The regular procedure for making micro-scale agarose gel microbeads appears to be an excellent way to manufacture systematic homogeneous gel environments.

There are three results for dynamics in the nanoscale gel environment. First, for the case of spherical polysaccharide (Ficoll70) nanoparticles, the diffusivity is in agreement with the Ogston model with no free parameter. Second, the ratio of bulk-to-microbead diffusivity of water is approximately a factor of 100, suggesting the presence of large water pockets in the bulk agarose. Finally, the relative diffusivity in agarose (with respect to its value in water), as a function of the molecular weight of a flexible (PEG) polymer, is constant in the case of the encapsulated (microbead) agarose, but the corresponding ratio in bulk agarose shows an increase with increasing molecular weight.

How can these results be consistent? While we are simply reporting the experimental observations here, we offer a conjecture that is consistent with these results. If the bulk gel is more heterogeneous, then it contains regions with larger pores (*i.e.*, water pockets). This results in the larger values for

the measured water self-diffusivity. At the same time, it is feasible that the macromolecules, Ficoll70 and PEG, preferentially partition into the bulk gel's agarose-rich regions when the hydrodynamic radius is smaller than the pore size, but preferentially reside in the water pockets when R_H exceeds the pore size. At a given Φ_A, the agarose-rich regions have a smaller pore size, and hence result in lower self-diffusivity due to the increased confinement.

Regardless of whether the above picture is correct, one issue is clear. The agarose in the hierarchical nanoscale/microbead environment shows clean agreement with a simple model (for the spherical Ficolls), shows a low diffusivity for water consistent with fully confined water, and shows consistent molecular-weight-dependent scaling behaviour for flexible chainlike polymer in pure water and in the presence of confinement. Nanoscale confinement is achieved *via* control of the pore size of the gel in a range between 60 nm and 380 nm. Examination of larger and/or more complex macromolecules that have more direct biophysical relevance is our next target.

Conflicts of interest

There are no conflicts to declare.

Appendix A

A.1 Micro-scale drop generation

We used the co-flowing method to generate stable and mono-disperse water-in-oil emulsions in a glass microcapillary device. As shown in Fig. 9, we produce uniform droplets with wide range of size using 3 tip diameters: (a–d) $D_{tip} = (15 \pm 0.2)$ μm; (e–h) $D_{tip} = (19 \pm 0.4)$ μm; (i–l) $D_{tip} = (26 \pm 0.5)$ μm. The key size-controlling factor is the flow of the continuous (oil) phase that
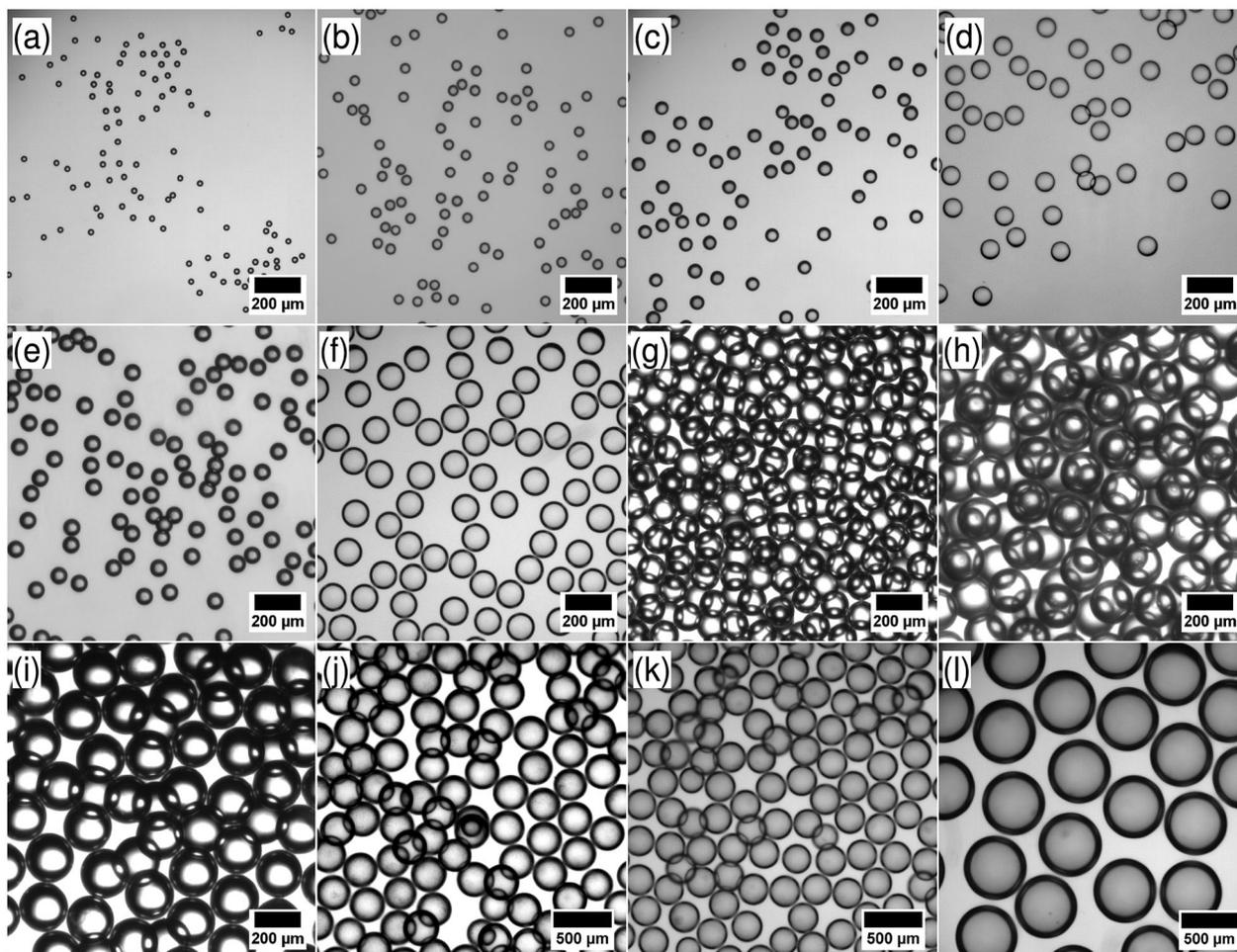
Fig. 9 Stable and monodisperse droplets: monodisperse water-in-oil emulsion of different droplet sizes are generated in microfluidic device. These droplets were verified to be stable for at least 26 hours. Droplet radius are: (a) (13.7 ± 0.2) μm; (b) (23.2 ± 0.4) μm; (c) (30 ± 0.6) μm; (d) (42 ± 0.8) μm; (e) (38.2 ± 0.4) μm; (f) (59 ± 1) μm; (g) (62 ± 2) μm; (h) (91 ± 3) μm; (i) (107 ± 2) μm; (j) (146 ± 3) μm; (k) (126 ± 3) μm; (l) (265 ± 4) μm. In all cases shown, the drops were stabilized with silica nanoparticles, as described in the text.
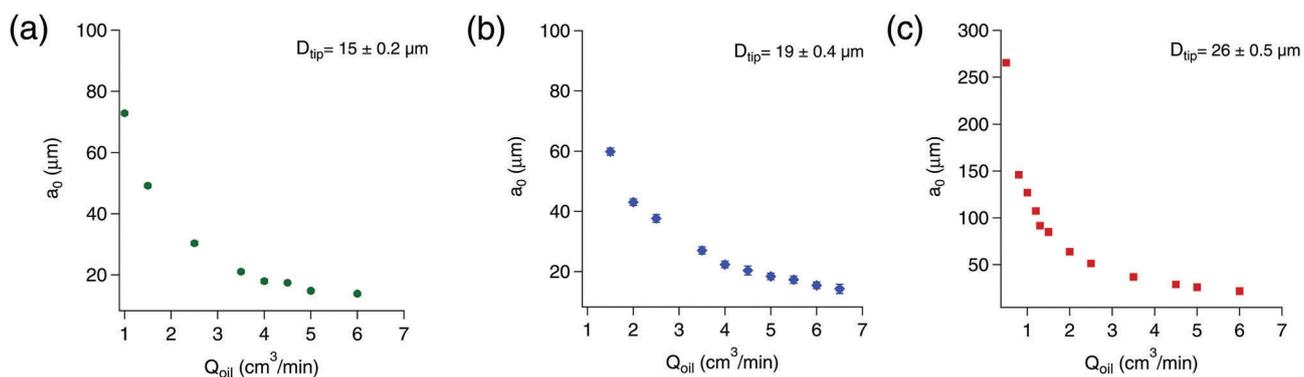
Fig. 10 Control of drop size: dependence of the mean radius, a_0, measured *via* image processing of optical micrographs, as a function of oil flow rate Q_{oil} for various tip diameters D_{tip}. (a) D_{tip} = 15 ± 0.2 μm, (b) D_{tip} = 19 ± 0.4 μm, (c) D_{tip} = 26 ± 0.5 μm. The examples shown are for silica-nanoparticle stabilized suspensions.

has been altered in a controlled manner. This results in monodisperse droplets whose size can be tuned.

The effect of flow rates on droplet size has been measured using bright field microscopy. In Fig. 10, droplet radius is

plotted as a function of increasing oil flow rate. Here we note the fact that at higher flow rates, droplet size decreases up to a point where the droplet radius approaches to the tip diameter of the inner capillary.

A.2 Relative pore sizes in agarose gel

The relative pore sizes $P(\Phi_A) = R_{pore}/R_{pore}(\Phi_A = 0.02)$ in agarose microbeads were determined precisely. These values are tabulated in Table 1 in order to serve as a look-up table.

Acknowledgements

References

1 D. Boal, *Mechanics of the Cell*, Cambridge University Press, 2012.

2 A. B. Fulton, *Cell*, 1982, **30**, 345–347.

3 R. J. Ellis, *Trends Biochem. Sci.*, 2001, **26**, 597–604.

4 D. S. Tawfik and A. D. Griffiths, *Nat. Biotechnol.*, 1998, **16**, 652–656.

5 X.-Y. Wang, Y. Pei, M. Xie, Z.-H. Jin, Y.-S. Xiao, Y. Wang, L.-N. Zhang, Y. Li and W.-H. Huang, *Lab Chip*, 2015, **15**, 1178–1187.

6 I. K. Zervantonakis, S. K. Hughes-Alford, J. L. Charest, J. S. Condeelis, F. B. Gertler and R. D. Kamm, *Proc. Natl. Acad. Sci. U. S. A.*, 2012, **109**, 13515–13520.

7 L. Shang, Y. Cheng and Y. Zhao, *Chem. Rev.*, 2017, **117**, 7964–8040.

8 L. Rosenfeld, T. Lin, R. Derda and S. K. Tang, *Microfluid. Nanofluid.*, 2014, **16**, 921–939.

9 J. Clausell-Tormos, D. Lieber, J.-C. Baret, A. El-Harrak, O. J. Miller, L. Frenz, J. Blouwolff, K. J. Humphry, S. Köster and H. Duan, *et al.*, *Chem. Biol.*, 2008, **15**, 427–437.

10 E. Brouzes, M. Medkova, N. Savenelli, D. Marran, M. Twardowski, J. B. Hutchison, J. M. Rothberg, D. R. Link, N. Perrimon and M. L. Samuels, *Proc. Natl. Acad. Sci. U. S. A.*, 2009, **106**, 14195–14200.

11 J.-u. Shim, L. F. Olguin, G. Whyte, D. Scott, A. Babtie, C. Abell, W. T. Huck and F. Hollfelder, *J. Am. Chem. Soc.*, 2009, **131**, 15251–15256.

12 J.-C. Baret, O. J. Miller, V. Taly, M. Ryckelynck, A. El-Harrak, L. Frenz, C. Rick, M. L. Samuels, J. B. Hutchison and J. J. Agresti, *et al.*, *Lab Chip*, 2009, **9**, 1850–1858.

13 L. Kisley, K. A. Serrano, D. Guin, X. Kong, M. Gruebele and D. E. Leckband, *ACS Appl. Mater. Interfaces*, 2017, **9**, 21606–21617.

14 G. Karoubi, M. L. Ormiston, D. J. Stewart and D. W. Courtman, *Biomaterials*, 2009, **30**, 5445–5455.

15 A. Hayashi and T. Kanzaki, *Food Hydrocolloids*, 1987, **1**, 317–325.

16 A. G. Carlos, Y. Teramura and H. Iwata, *Transplantation*, 2009, **87**, 29–34.

17 D. Pelaez, C.-Y. Charles Huang and H. S. Cheung, *Stem Cells Dev.*, 2009, **18**, 93–102.

18 O. Bonhomme, J. Leng and A. Colin, *Soft Matter*, 2012, **8**, 10641–10649.

19 L. Yobas, S. Martens, W.-L. Ong and N. Ranganathan, *Lab Chip*, 2006, **6**, 1073–1079.

20 T. Nisisako and T. Torii, *Lab Chip*, 2008, **8**, 287–293.

21 T. Thorsen, R. W. Roberts, F. H. Arnold and S. R. Quake, *Phys. Rev. Lett.*, 2001, **86**, 4163.

22 D. Link, S. L. Anna, D. Weitz and H. Stone, *Phys. Rev. Lett.*, 2004, **92**, 054503.

23 S. L. Anna, N. Bontoux and H. A. Stone, *Appl. Phys. Lett.*, 2003, **82**, 364–366.

24 A. Woodward, T. Cosgrove, J. Espidel, P. Jenkins and N. Shaw, *Soft Matter*, 2007, **3**, 627–633.

25 P. Umbanhowar, V. Prasad and D. Weitz, *Langmuir*, 2000, **16**, 347–351.

26 A. S. Utada, A. Fernandez-Nieves, J. M. Gordillo and D. A. Weitz, *Phys. Rev. Lett.*, 2008, **100**, 014502.

27 J.-C. Baret, *Lab Chip*, 2012, **12**, 422–433.

28 B. Binks and S. Lumsdon, *Langmuir*, 2001, **17**, 4540–4547.

29 R. Miller, V. Fainerman, V. Kovalchuk, D. Grigoriev, M. Leser and M. Michel, *Adv. Colloid Interface Sci.*, 2006, **128**, 17–26.

30 S. Arnott, A. S. W. E. Fulmer, W. E. Scott, I. C. M. Dea, R. Moorhouse and D. A. Rees, *J. Mol. Biol.*, 1974, **90**, 269–284.

31 E. M. Johnson, D. A. Berk, R. K. Jain and W. M. Deen, *Biophys. J.*, 1996, **70**, 1017–1023.

32 S. Waki, J. Harvey and A. Bellamy, *Biopolymers*, 1982, **21**, 1909–1926.

33 G. A. Griess, E. T. Moreno, R. A. Easom and P. Serwer, *Biopolymers*, 1989, **28**, 1475–1484.

34 G. A. Griess, K. B. Guiseley and P. Serwer, *Biophys. J.*, 1993, **65**, 138–148.

35 E. M. Johnson, D. A. Berk, R. K. Jain and W. M. Deen, *Biophys. J.*, 1995, **68**, 1561–1568.

36 N. Pernodet, M. Maaloum and B. Tinland, *Electrophoresis*, 1997, **18**, 55–58.

37 M. Maaloum, N. Pernodet and B. Tinland, *Electrophoresis*, 1998, **19**, 1606–1610.

38 A. Pluen, P. A. Netti, R. K. Jain and D. A. Berk, *Biophys. J.*, 1999, **77**, 542–552.

39 J. P. Gong, N. Hirota, A. Kakugo, T. Narita and Y. Osada, *J. Phys. Chem. B*, 2000, **104**, 9904–9908.

40 N. Fatin-Rouge, K. Starchev and J. Buffle, *Biophys. J.*, 2004, **86**, 2710–2719.

41 W. Deen, *AIChE J.*, 1987, **33**, 1409–1425.

42 A. Ogston, B. Preston and J. Wells, *Proc. R. Soc. London, Ser. A*, 1973, 297–316.

43 D. Sandrin, D. Wagner, C. Sitta, R. Thoma, S. Felekyan, H. Hermes, C. Janiak, N. de Sousa Amadeu, R. Kühnemuth and H. Löwen, *et al.*, *Phys. Chem. Chem. Phys.*, 2016, **18**, 12860–12876.

44 M. Moussaoui, M. Benlyas and P. Wahl, *J. Chromatogr. A*, 1992, **591**, 115.

45 J. Tong and J. L. Anderson, *Biophys. J.*, 1996, **70**, 1505–1513.

46 C. D'Agostino, R. Liuzzi, L. F. Gladden and S. Guido, *Soft Matter*, 2017, **13**, 2952–2961.

47 J. Meyer and M. Scholz, Fumed silanized silica, *US Pat.*, 8211971, 2012.

48 P. Callaghan, K. Jolley and R. Humphrey, *J. Colloid Interface Sci.*, 1983, **93**, 521–529.

49 S. Barhoum, S. Palit and A. Yethiraj, *Prog. Nucl. Magn. Reson. Spectrosc.*, 2016, **94**, 1–10.

50 J. E. Tanner, *J. Chem. Phys.*, 1970, **52**, 2523–2526.

51 A. M. Gañán-Calvo and J. M. Gordillo, *Phys. Rev. Lett.*, 2001, **87**, 274501.

52 M. Sun, S. S. Bithi and S. A. Vanapalli, *Lab Chip*, 2011, **11**, 3949–3952.

53 C. A. Stan, S. K. Tang and G. M. Whitesides, *Anal. Chem.*, 2009, **81**, 2399–2402.

54 H. Fan and A. Striolo, *Phys. Rev. E: Stat., Nonlinear, Soft Matter Phys.*, 2012, **86**, 051610.

55 J. R. Wenner and V. A. Bloomfield, *Biophys. J.*, 1999, **77**, 3234–3241.

56 S. Palit, L. He, W. A. Hamilton, A. Yethiraj and A. Yethiraj, *Phys. Rev. Lett.*, 2017, **118**, 097801.

57 J. J. Sahlin and N. A. Peppas, *Macromolecules*, 1996, **29**, 7124–7129.

58 C. I. Bica, R. Borsali, E. Geissler and C. Rochas, *Macromolecules*, 2001, **34**, 5275–5279.

59 S. Kwak and M. Lafleur, *Colloids Surf., A*, 2003, **221**, 231–242.

60 I. Sebti, D. Blanc, A. Carnet-Ripoche, R. Saurel and V. Coma, *J. Food Eng.*, 2004, **63**, 185–190.

61 B. Amsden, *Macromolecules*, 1998, **31**, 8382–8395.

62 M. Djabourov, A. Clark, D. Rowlands and S. Ross-Murphy, *Macromolecules*, 1989, **22**, 180–188.

63 J. Narayanan, J.-Y. Xiong and X.-Y. Liu, *J. Phys.: Conf. Ser.*, 2006, 83.

64 J. Chou, A. Lennart, J. Wong, M. F. Ali, P. N. Floriano, N. Christodoulides, J. Camp and J. T. McDevitt, *Anal. Chem.*, 2012, **84**, 2569–2575.

65 M. Doi and S. F. Edwards, *The Theory of Polymer Dynamics*, Oxford University Press, 1988, vol. 73.

66 P. A. Netz and T. Dorfmüller, *J. Chem. Phys.*, 1995, **103**, 9074–9082.